

Probabilistic Fault-Tolerant Universal Quantum Computation and Sampling Problems in Continuous Variables

Tom Douce¹, Damian Markham², Elham Kashefi^{1,2}, Peter van Loock³, Giulia Ferrini^{3,4}

¹ *School of Informatics, University of Edinburgh,*

10 Crichton Street, Edinburgh, EH8 9AB, United Kingdom

² *Sorbonne Université, CNRS, Laboratoire d'Informatique de Paris 6, F-75005 Paris, France*

³ *Institute of Physics, Johannes-Gutenberg Universität Mainz, Staudingerweg 7, 55128 Mainz, Germany*

⁴ *Department of Microtechnology and Nanoscience (MC2),*

Chalmers University of Technology, SE-412 96 Gothenburg, Sweden

(Dated: December 14, 2024)

Continuous-Variable (CV) devices are a promising platform for demonstrating large-scale quantum information protocols. In this framework, we define a general quantum computational model based on a CV hardware. It consists of vacuum input states, a finite set of gates – including non-Gaussian elements – and homodyne detection. We show that this model incorporates encodings sufficient for probabilistic fault-tolerant universal quantum computing. Furthermore, we show that this model can be adapted to yield sampling problems that cannot be simulated efficiently with a classical computer, unless the polynomial hierarchy collapses. This allows us to provide a simple paradigm for short-term experiments to probe quantum advantage relying on Gaussian states, homodyne detection and some form of non-Gaussian evolution. We finally address the recently introduced model of Instantaneous Quantum Computing in CV, and prove that the hardness statement is robust with respect to some experimentally relevant simplifications in the definition of that model.

PACS numbers:

I. Introduction

Continuous Variable (CV) systems are emerging as promising candidates for the implementation of quantum computation (QC) models. The main reason for this interest relies in the possibility of generating deterministically large resource states such as cluster states, composed of up to one million modes [1]. More generally, the optical CV approach includes highly efficient ways to prepare and measure sophisticated quantum states. Furthermore, new experimental techniques that are not anymore purely optical are being addressed for CV quantum information, based e.g. on microwaves resonators coupled to superconducting Josephson junctions [2], or on opto-mechanical resonators [3, 4].

In contrast to their typically high efficiencies, optical CV schemes suffer from an intrinsic sensitivity to Gaussian errors such as photon loss and thermal noise. Standard approaches to quantum error correction, encoding a logical mode into many physical modes, have been proven to be inefficient when both the error itself and the operations for error correction are of Gaussian nature [5, 6]. Nonetheless, codes have been proposed that can protect logical qubits encoded into one or more optical modes against errors induced, for instance, from photon loss [7–15]. In particular, those schemes encoding discrete logical information into a single optical mode, such as the so-called cat codes [12–15], are sometimes referred to as CV codes. The very first proposal of such a CV code is the famous Gottesmann-Kitaev-Preskill (GKP) encoding that later has been shown to allow for universal fault-tolerant quantum computation in the measurement-based scenario [16, 17]. This encoding uses highly non-Gaussian

states, the so-called GKP states, in order to encode DV quantum information on a CV hardware, namely onto the infinite dimensional Hilbert space of a single harmonic oscillator. These states possess a comb-like wavefunction, with peaks equally spaced placed either at even (resp. odd) multiples of $\sqrt{\pi}$ for the 0-logical state (resp. 1-logical state). GKP states have also been used as ancillary input states in a recently defined sampling model in CV, namely IQP [18], whose output probability distribution was shown to be hard to sample. However, these states are highly impractical to produce, and only recently their experimental generation has been tackled [19]. This practical difficulty makes it desirable to define both a model of fault-tolerant CV quantum computation and sampling models that are hard to classically simulate, which do not explicitly require GKP states as ancillary states at the input of the model.

In this work we address these two aspects. On the one hand, we define a model for universal fault-tolerant quantum computation in CV where GKP states are probabilistically generated within the model itself. Similar to the original version of an in-principle efficient, universal and to some extent fault-tolerant, linear-optics quantum computer based on probabilistic quantum gates with single-photon states, the well-known KLM model [20], our model as presented here is also intended as an especially conceptual step forward rather than an immediately implementable proposal. In this sense, our model is not intended to be of immediate practical use, since its success probabilities may be too low to yield an experimentally viable and scalable solution for universal quantum computation. It allows us to show that in principle a number of ancillary modes set in the vacuum state, a polynomial number of gates drawn from an elementary

gate set and homodyne detection are sufficient for probabilistic universal fault-tolerant quantum computation. Compared to Ref. [21], we show that a finite set of gates, characterized by specific values of the gate parameters rather than a continuum, is sufficient for CV quantum computing with vacuum states.

On the other hand, we later specialize to sampling models and show that models that are hard to classically sample up to relative error can be defined, where no GKP state is needed at the input, thereby improving the results of Ref. [18] and obtaining more experimentally-friendly architectures. These models are solely based on homodyne detection for the required measurements.

As a common ground for both applications, we provide an explicit protocol for the probabilistic generation of GKP states, by starting from vacua, a given set of elementary quantum gates and using homodyne detection. This generation method is based on the protocol of Ref. [22], that uses input squeezed cat states, beamsplitters and homodyne measurements. We further provide an explicit decomposition of the cross-Kerr interaction necessary to generate the cat states in terms of elementary gates that belong to our models. In this way, GKP generation is subsumed within the models themselves. As an important point, the definition of the gates in our models depends on the tolerated error probability on the computation result.

The paper is structured as follows. In Sec. II we recall the basics of GKP encoding. In Sec. III we set the problem and define in more detail the models we are interested in. Section IV is dedicated to the description and characterization of the specific protocol used to generate GKP states. Then Sections V and VI discuss the issues of fault-tolerance and its implications in the universal as well as in the subuniversal sampling models. Finally conclusions and perspectives are presented in Section VII. Throughout the paper we adopt the convention $[\hat{q}, \hat{p}] = i$ for the quadratures commutator, which corresponds to the relation $\hat{a} = (\hat{q} + i\hat{p})/\sqrt{2}$ and fixes the vacuum fluctuations to $\Delta^2 q_0 \equiv \Delta^2 p_0 = 1/2$.

II. Recalling the GKP encoding

GKP states are highly non-Gaussian states with a comb-like wavefunction. They allow to encode a qubit into a harmonic oscillator's Hilbert space. Ideal GKP states, that we denote as $|0_L\rangle, |1_L\rangle$, are defined as wavefunctions made of an infinite number of Dirac peaks [16]:

$$\begin{aligned} |0_L\rangle &= \sum_n |2n\sqrt{\pi}\rangle_q = \sum_n |n\sqrt{\pi}\rangle_p, \\ |1_L\rangle &= \sum_n |(2n+1)\sqrt{\pi}\rangle_q = \sum_n (-1)^n |n\sqrt{\pi}\rangle_p. \end{aligned} \quad (1)$$

These states realize a one-to-one correspondence between simple qubit operations and Gaussian transformations. More formally, the Clifford group is mapped to Gaussian

transformations as follows:

$$e^{i\sqrt{\pi}\hat{q}} \rightarrow \hat{Z}, \quad e^{i\hat{q}_1\hat{q}_2} \rightarrow \hat{C}_Z, \quad \hat{F} = e^{i\frac{\pi}{4}(\hat{p}^2 + \hat{q}^2)} \rightarrow \hat{H}, \quad (2)$$

while the \hat{T} gate is mapped as

$$e^{i\frac{\pi}{4}\left[2\left(\frac{\hat{q}}{\sqrt{\pi}}\right)^3 + \left(\frac{\hat{q}}{\sqrt{\pi}}\right)^2 - 2\frac{\hat{q}}{\sqrt{\pi}}\right]} \rightarrow \hat{T}. \quad (3)$$

Realistic logical qubit states, that we indicate with $|0_G\rangle, |1_G\rangle$, are instead normalizable states, accounting for finite squeezing. Each Dirac peak is replaced by a normalized Gaussian of width σ , while the infinite sum itself becomes a Gaussian envelope function of width δ^{-1} (see Figure 1). Because of this and despite the fact that they are highly non-Gaussian states, we will refer to these states as Gaussian GKP states in the following. The resulting wavefunctions are:

$$\begin{aligned} \langle q|0_G\rangle &= \int dudv G(u)F(v)e^{-iu\hat{p}}e^{-iv\hat{q}}\langle q|0\rangle_L \\ &= N_0 \sum_n \exp\left(-\frac{(2n)^2\pi\delta^2}{2}\right) \exp\left(-\frac{(q-2n\sqrt{\pi})^2}{2\sigma^2}\right), \end{aligned} \quad (4)$$

$$\begin{aligned} \langle q|1_G\rangle &= \int dudv G(u)F(v)e^{-iu\hat{p}}e^{-iv\hat{q}}\langle q|1\rangle_L \\ &= N_1 \sum_n \exp\left(-\frac{(2n+1)^2\pi\delta^2}{2}\right) \exp\left(-\frac{(q-(2n+1)\sqrt{\pi})^2}{2\sigma^2}\right), \end{aligned} \quad (5)$$

where we have introduced the noise distributions

$$G(u) = \frac{1}{\sigma\sqrt{2\pi}}e^{-\frac{u^2}{2\sigma^2}}; \quad F(v) = \frac{1}{\delta\sqrt{2\pi}}e^{-\frac{v^2}{2\delta^2}}, \quad (6)$$

and N_0 and N_1 are normalization constants. In the following, for conceptual clarity as well as simplicity, we consider symmetric GKP states, which have symmetric noise properties in the two quadratures, and are characterized by $\sigma = \delta$.

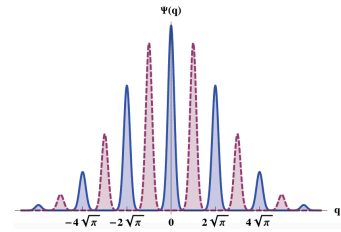


FIG. 1: Wavefunction in position representation of the GKP $|0_G\rangle$ state in continuous blue ($|1_G\rangle$ in dashed red) with $\delta = 0.25$ from Equation (4).

Ancillary $|0_G\rangle$ GKP states serve as resources to achieve fault-tolerance in CV [16, 17]. The idea in [16] is to entangle the state to be corrected at a given step of the computation with an ancillary GKP state, and then measure the ancillary modes by means of homodyne detection. One can show that in this way the noise in the \hat{q} quadrature of a GKP encoded quantum state can be replaced by the noise of the ancillary $|0_G\rangle$ state. Repeating this gadget after a Fourier transform allows for correction of the other quadrature, thereby keeping the error below a desired amount. In Sec. V we address in detail how this error correction procedure can be used in order to ensure fault-tolerance in our model.

III. Definition of the models

In this section we define the quantum computational models we are interested in. We first describe the CV universal quantum computational model. Then, we turn to subuniversal models and define the corresponding sampling problems.

A. Probabilistic universal fault-tolerant quantum computation in CV

We first address our model for probabilistic, universal and fault-tolerant quantum computing in CV. It is based upon the following elements:

- (i) the multimode input state is initialized in the vacuum $|0\rangle^{\otimes m}$, where m is the total number of modes;
- (ii) the gates composing the circuit are drawn from the following finite sets:

$$A_1 = \left\{ e^{i\hat{d}\hat{q}}, e^{i\hat{s}\hat{q}^2}, e^{i\hat{c}\hat{q}^3}, e^{i\hat{b}\hat{q}_1\hat{q}_2} \right\}, \quad (7)$$

$$A_2 = \left\{ e^{i\hat{q}\sqrt{\pi}}, e^{i\frac{\pi}{4}(\hat{p}^2 + \hat{q}^2)}, e^{i\hat{q}_1\hat{q}_2}, e^{i\frac{\pi}{4}\left[2\left(\frac{\hat{q}}{\sqrt{\pi}}\right)^3 + \left(\frac{\hat{q}}{\sqrt{\pi}}\right)^2 - 2\frac{\hat{q}}{\sqrt{\pi}}\right]} \right\}, \quad (8)$$

where the parameters in A_1 will be fixed later. They will be determined by the desired precision on the computation result. Note that, in contrast to Ref. [21], the CV gates in Eqs.(7) and (8) are characterized by specific values of the gate parameters, instead of spanning the full real axis. The linear and quadratic gates in Eqs.(7) and (8) are generally regarded as experimentally feasible. A non-Gaussian, experimentally challenging gate has also been included to A_1 (with powers greater than 2 in \hat{q} and/or \hat{p}), and a similar non-Gaussian gate appears in A_2 ;

(iii) the measurements are done via homodyne detection in the momentum quadrature, i.e. by measuring \hat{p} , which corresponds to approximately measuring in the GKP basis $\{|+/-_G\rangle\}$ [16]. The homodyne detection may have a finite resolution, which is modeled by the finitely-resolved \hat{p}^η operator defined as [18, 23]

$$\hat{p}^\eta = \sum_{k=-\infty}^{\infty} p_k \int_{-\infty}^{\infty} dp \chi_k^\eta(p) |p\rangle\langle p| \equiv \sum_{k=-\infty}^{\infty} p_k \hat{P}_k \quad (9)$$

with $\chi_k^\eta(p) = 1$ for $p \in [p_k - \eta, p_k + \eta]$ and 0 outside, $p_k = 2\eta k$ and 2η the resolution, associated with the width of the detector pixels. As a technical remark, note that, provided that we can find an integer K such that $\sqrt{\pi} = K\eta$, this binning is consistent with the dichotomy at the level of logical measurements.

We prove that this model is at least as powerful as the standard qubit-based quantum computers by showing that any BQP [41] instance decided by a quantum circuit working with qubits can be mapped to a probabilistic CV circuit with a constant overhead. As mentioned above, the mapping relies on the ability to encode qubits in a quantum harmonic oscillator through the GKP procedure. More specifically we first have to generate (probabilistically) the GKP qubits in CV by applying the gate set A_1 upon several vacuum states. Then we use the gate set A_2 : it is the exact analog of the universal DV gate set in the subspace spanned by the GKP states $\{|0/1_G\rangle\}$ – as presented in Eqs.(2) and (3).

B. Subuniversal models and sampling

Beyond fault-tolerant universal quantum computation, we address two subuniversal models of quantum computation that are associated to two respective sampling problems.

1. CV random circuit sampling

The first subuniversal model that we consider is represented in Fig.2. This family of circuits share the same elementary

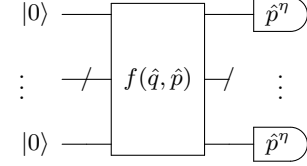


FIG. 2: Sampling with Gaussian input state and homodyne detection. The finitely-resolved homodyne measurement \hat{p}^η has resolution 2η .

gates as the universal model defined in Sec.III A, namely the gate sets A_1 (7) and A_2 (8).

In analogy to the family of circuits with random gates drawn from an elementary set for qubits, we refer to this architecture as to CV random circuit sampling [24]. Finite resolution in the homodyne detection ensures that we can associate well-defined probabilities to the continuous measurement outcomes through binning. Note that the detection modeled in Eq.(9) is equivalent to perfectly resolved homodyne detectors followed by a discretization (binning) of the measurement outcomes.

This model is not universal anymore, since the randomness occurring at the level of the measurement is not counteracted by post-selection. Nevertheless, we show that exact sampling – or equivalently up to relative error – from the probability distribution of the measurement outcomes of the circuit family represented in Fig.2 is classically hard, in the worst case scenario.

2. CV Instantaneous Quantum Computing with input squeezed states

The second subuniversal model we are interested in is Instantaneous Quantum Computing in CV (Fig.3).

This model is composed of the same elementary gates as those of the model in Fig.2, except for the Fourier transform, namely

$$\tilde{A}_1 = \left\{ e^{i\tilde{d}\hat{q}} e^{i\tilde{b}\hat{q}_1\hat{q}_2}, e^{i\tilde{s}\hat{q}^2}, e^{i\tilde{c}\hat{q}^3} \right\}, \quad (10)$$

$$\tilde{A}_2 = \left\{ e^{i\tilde{q}\sqrt{\pi}}, e^{i\tilde{q}_1\hat{q}_2}, e^{i\frac{\pi}{4}\left[2\left(\frac{\tilde{q}}{\sqrt{\pi}}\right)^3 + \left(\frac{\tilde{q}}{\sqrt{\pi}}\right)^2 - 2\frac{\tilde{q}}{\sqrt{\pi}}\right]} \right\}. \quad (11)$$

Therefore, all the gates in this model are diagonal in the position representation. We require momentum squeezed states $|\sigma\rangle$ to be present at the input. This model is a simpler version than the one introduced in Ref. [18]. Specifically we show here

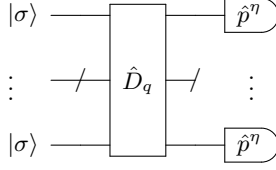


FIG. 3: IQP circuit in CVs. $|\sigma\rangle$ are finitely squeezed states with variance σ in the \hat{p} representation. The gate \hat{D}_q is a uniform combination of elementary gates from the set in Eqs.(10) and (11). The finitely-resolved homodyne measurement \hat{p}^η has resolution 2η .

that (i) we do not need GKP states as resource states and (ii) the squeezing parameter in the input states is constant and does not depend on the circuit size. These features make the present model more experimentally realistic, and yet we will prove that it retains its classical hardness (again for the exact probability distribution, and in the worst-case scenario).

The proofs of computational hardness for both sampling models, as well as the universality of the computational model presented in Sec.III A, will be based on the ability to synthesize GKP states by means of a sequence of the elementary gates that belong to the models themselves. To this end, in the following section we show how the approximate GKP states generation can be decomposed in terms of elementary gates.

IV. Approximate GKP states from a finite set of CV gates

In this section we provide a protocol for the probabilistic generation of approximate GKP states. More precisely, the main result we prove in this section is that there exists a finite number of CV gates that combined together allow one to generate approximate GKP states using vacuum input states and homodyne detection.

Our protocol for GKP generation can be divided in two steps: 1) probabilistic generation of cat states from vacuum; 2) probabilistic generation of approximate GKP states from cat states. The former protocol is based on that of Ref. [25] and on gate decomposition [26] and squeezing amplification [27], while the latter is based on Ref. [22]. We detail first step 2 and later step 1 here below, focussing on the respective associated fidelities and success probabilities. The following subsections are rather technical and the uninterested reader may skip them and move to Sec.V where we take advantage of this protocol.

A. GKP states from cat states

The protocol designed by Vasconcelos and co-authors in [22] relies on squeezed cat states combined in a linear optical network and measured by homodyne detection. The basic idea is (i) prepare two cat states $|\alpha\rangle + |-\alpha\rangle$ of real amplitude α (ii) squeeze them to reproduce the squeezing of the peaks in a GKP state (iii) send them to a balanced BS (iv) measure the \hat{p} quadrature of one of the modes. If the outcome of the homodyne detection is 0, the output state is a state containing

three Gaussian peaks enveloped by a binomial distribution, i.e. a *binomial state*, that approximates a GKP state. We will refer to these states as to binomial GKP states in what follows. The first iteration of this scheme is represented in Fig. 4. This scheme can then be repeated to produce higher

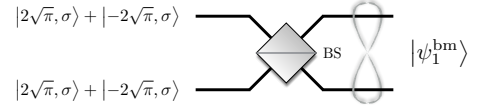


FIG. 4: First iteration of the protocol of Ref. [22] for the probabilistic generation of binomial states: two cat states are squeezed, then combined at a beamsplitter. The \hat{p} quadrature is then measured in one of the output modes.

order binomial states possessing a larger number of peaks, better approximating Gaussian GKP states. More specifically, the m th binomial GKP state's position wavefunction reads:

$${}_q\langle q|0_m\rangle = \frac{\pi^{-1/4}}{\sqrt{\binom{2^{m+1}}{2^m}\sigma}} \sum_{i=0}^{2^m} \binom{2^m}{i} e^{-\frac{(q-2\sqrt{\pi}(i-2^{m-1}))^2}{2\sigma^2}}, \quad (12)$$

where σ characterizes the squeezing of each peak. In general, let m be a positive integer. We set the amplitude of the cat states to $\alpha_m = \sqrt{2^{m-1}}\sqrt{\pi}\sigma^{-1}$, where σ corresponds to the amount of squeezing of the individual peaks in the GKP position wavefunction.

1. Quantification of the quality of the binomial GKP states

We compare the binomial GKP states obtained through this procedure to the standard Gaussian GKP states in Eq. (1). We stress that in a binomial state, although the individual peaks are standard Gaussians, the envelope is described by binomial coefficients. More specifically, the weight of the i -th peak, in terms of probabilities, is given by

$$\frac{1}{\binom{2^{m+1}}{2^m}} \binom{2^m}{i}^2 \quad (13)$$

instead of the Gaussian function characterized by a squeezing parameter given in Eq.(4). We aim at finding the closest Gaussian function approximating the distribution in Eq. (13). Using the central limit theorem in the limit of large m , the binomial distribution of parameters 2^m and $1/2$ leads to a normal distribution of mean 2^{m-1} and variance 2^{m-2} . Mathematically it means we have the following relation:

$$\frac{1}{2^{2^n}} \binom{2^m}{i}^2 \approx \frac{1}{\sqrt{2\pi 2^{m-2}}} \exp\left(-\frac{(2^{m-1}-i)^2}{2 \cdot 2^{m-2}}\right). \quad (14)$$

So necessarily the distribution in Eq. (13), which corresponds to the left-hand-side squared, will be associated with a Gaussian of mean 2^{m-1} and variance 2^{m-3} . Taking into account the proper normalisation we obtain:

$$\frac{1}{\binom{2^{m+1}}{2^m}} \binom{2^m}{i}^2 \approx \frac{1}{\sqrt{2\pi 2^{m-3}}} \exp\left(-\frac{(2^{m-1}-i)^2}{2 \cdot 2^{m-3}}\right). \quad (15)$$

In a standard, Gaussian enveloped GKP state, recall from Eq. (4) that the weight reads $\exp(-(2j\sqrt{\pi})^2\sigma^2/2)$ for the j -th peak of the wavefunction. Using Eq. (14) it yields for the corresponding squeezing parameter σ :

$$\sigma^2 = \frac{1}{2^m \pi}. \quad (16)$$

We stress that due to Eq.(16) the effective squeezing in the binomial GKP states depends on the number of iterations of the protocol: the higher the number of iterations, the higher the squeezing. Thus we have identified the closest Gaussian GKP state to the binomial GKP state of Eq. (13). Its position wavefunction reads:

$${}_q\langle q|0_G\rangle = \frac{(2^{m-2})^{-1/4}}{\sqrt{\sigma\pi}} \sum_{j=-\infty}^{+\infty} e^{-\frac{(2j\sqrt{\pi})^2}{2 \cdot 2^m \pi}} e^{-\frac{(q-2j\sqrt{\pi})^2}{2\sigma^2}}. \quad (17)$$

We may now compute the fidelity between the binomial state produced through the protocol of Ref. [22] and the Gaussian GKP state. To simplify the calculations we assume that the Gaussian peaks are narrow enough to be considered as orthogonal. The inner product thus reads:

$$|\langle 0_m|0_G\rangle| \approx \frac{\pi^{-1/4} (2^{m-2})^{-1/4}}{\sqrt{\binom{2^{m+1}}{2^m}}} \sum_{i=0}^{2^m} \sum_{j=-\infty}^{+\infty} \binom{2^m}{i} e^{-\frac{(2j\sqrt{\pi})^2}{2 \cdot 2^m \pi}} \int dq \frac{1}{\sqrt{\pi}\sigma} e^{-\frac{(q-2\sqrt{\pi}(i-2^{m-1}))^2}{2\sigma^2}} e^{-\frac{(q-2j\sqrt{\pi})^2}{2\sigma^2}}. \quad (18)$$

This assumption also implies that the integral vanishes except for the $2^m + 1$ cases when $j = i - 2^{m-1}$, and it is then properly normalized. So we simply have to focus on the overlap of the envelopes, namely:

$$|\langle 0_m|0_G\rangle| \approx \frac{\pi^{-1/4} (2^{m-2})^{-1/4}}{\sqrt{\binom{2^{m+1}}{2^m}}} \sum_{i=0}^{2^m} \binom{2^m}{i} e^{-\frac{(i-2^{m-1})^2}{2^{m-1}}}. \quad (19)$$

Table 5 summarizes the results for different values of the iteration parameter m . Note that the fidelity between binomial and Gaussian GKP states becomes quite large already for few iterations.

m	Squeezing equivalent	Overlap with Gaussian GKP
1	5 dB	0.9976
2	8 dB	0.9986
3	11 dB	0.9997
4	14 dB	0.9999

FIG. 5: Comparison between binomial states and their closest Gaussian GKP counterpart. Recall that the number of peaks scales as $2^m + 1$.

2. Finite resolution and success probability

The protocol for GKP states synthesis from cat states that we have described above is probabilistic, and indeed it works only if all $2^m - 1$ homodyne detections yield outcome 0. In order for the success probability not to be 0, homodyne detection must have finite resolution. Hence, we introduce a

resolution η for the homodyne detection as a binning of the real axis, consistently with Eq.(9). The projector on outcome zero associated with all homodyne detections thus reads:

$$P_0^m = \int_{-\eta}^{\eta} ds |\mathbf{s}\rangle_p \langle \mathbf{s}|, \quad (20)$$

where \mathbf{s} is a $2^m - 1$ dimensional real vector and the integration is over the box $[-\eta, \eta]^{2^m - 1}$. In the following we quantify the success probability associated with GKP state synthesis using this detection binning.

We first focus on the 2^m mode quantum state $|\psi_m^{\text{bm}}\rangle$ right before the measurements are performed. We denote $|\alpha, \sigma\rangle$ a displaced squeezed state, where $\alpha \in \mathbb{R}$ corresponds to the displacement and σ to its squeezing. The position wavefunction of such a state is:

$${}_q\langle q|\alpha, \sigma\rangle = \frac{1}{\pi^{1/4} \sigma^{1/2}} \int dq e^{-\frac{(q - \sqrt{2}\alpha)^2}{2\sigma^2}}. \quad (21)$$

We consider as input state the squeezed cat state. With these notations, the input state $|\psi_m^{\text{in}}\rangle$ to generate the m th binomial state is merely:

$$|\psi_m^{\text{in}}\rangle = \frac{1}{\sqrt{N}} \bigotimes_{i=1}^{2^m} (|\alpha_m, \sigma\rangle_i + |-\alpha_m, \sigma\rangle_i), \quad (22)$$

where the subscript i labels the mode, $\alpha_m = \sqrt{2^{m-1}}\sqrt{\pi}$ and $N = [2(1 + e^{-2\alpha_m^2})]^{2^m}$. Note that, in this simple case, the action of a beamsplitter on two identically squeezed states reads:

$$|\mu, \sigma\rangle |\lambda, \sigma\rangle \xrightarrow{\text{BS}} \left| \frac{\mu - \lambda}{\sqrt{2}}, \sigma \right\rangle \left| \frac{\mu + \lambda}{\sqrt{2}}, \sigma \right\rangle. \quad (23)$$

So the global state after the beamsplitters is a sum of many 2^m -fold tensorial products involving displaced squeezed states. We can actually isolate the output mode and using combinatorial arguments finally write down $|\psi_m^{\text{bm}}\rangle$:

$$|\psi_m^{\text{bm}}\rangle = \frac{1}{\sqrt{N}} \sum_{i=-2^{m-1}}^{2^{m-1}} |2i\sqrt{\pi}, \sigma\rangle \sum_{j=1}^{\binom{2^m}{2^{m-1}+i}} |\alpha_1^{i,j}, \sigma\rangle \dots |\alpha_{2^m-1}^{i,j}, \sigma\rangle. \quad (24)$$

where the $\alpha_k^{i,j}$'s are multiples of $\sqrt{\pi}$ and bounded in absolute value by $2^{m-1}\sqrt{\pi}$.

Now recall that the momentum wavefunction of a displaced squeezed state of real amplitude reads:

$${}_p\langle s|\alpha, \sigma\rangle = \frac{\sqrt{\sigma}}{\pi^{1/4}} e^{-i\sqrt{2}\alpha s} e^{-\frac{s^2\sigma^2}{2}}. \quad (25)$$

Let ρ_r be the matrix obtained after tracing out the unmeasured mode. Starting from Eq. (24), we have (note the relabeling of the variables):

$$\rho_r = \frac{1}{N} \sum_{i=0}^{2^m} \sum_{j,j'=1}^{\binom{2^m}{i}} |\alpha_1^{i,j}, \sigma\rangle \dots |\alpha_{2^m-1}^{i,j}, \sigma\rangle \langle \alpha_1^{i,j'}, \sigma| \dots \langle \alpha_{2^m-1}^{i,j'}, \sigma|. \quad (26)$$

We may now derive the success probability of the protocol, i.e. the probability that $2^m - 1$ homodyne detections yield

outcome 0. In the state before the measurement, the maximum (absolute) value of all amplitudes is $2^{m-1}\sqrt{\pi}$. So if $\eta \cdot 2^{m-1}\sqrt{\pi} \ll 1$ and $\eta \cdot \sigma_m \ll 1$ we have from Eq. (25):

$${}_p\langle s | \alpha_k^{l,l'}, \sigma_m \rangle \approx \frac{\sqrt{\sigma_m}}{\pi^{1/4}}, \quad (27)$$

for all triples (k, l, l') and all $s \in [-\eta, \eta]$. The probability of hitting 0 for all measurements, $p_m(0)$, is then given by

$$p_m(0) = \text{Tr}(P_m(0)\rho_r) = \int_{-\eta}^{\eta} ds \langle s | \rho_r | s \rangle. \quad (28)$$

Using Eq. (27) we get:

$$\begin{aligned} p_m(0) &= \frac{1}{N} \int_{-\eta}^{\eta} ds \sum_{i=0}^{2^m} \sum_{j,j'=1}^{2^m} \left| \left(\frac{\sqrt{\sigma_m}}{\pi^{1/4}} \right)^{2^m-1} \right|^2 \\ &= \frac{1}{N} \int_{-\eta}^{\eta} ds \left(\frac{\sigma_m}{\sqrt{\pi}} \right)^{2^m-1} \sum_{i=0}^{2^m} \binom{2^m}{i}^2 \\ &= \frac{1}{N} (2\eta)^{2^m-1} \left(\frac{\sigma_m}{\sqrt{\pi}} \right)^{2^m-1} \binom{2^{m+1}}{2^m} \\ &= \frac{1}{2^{2^m}} \binom{2^{m+1}}{2^m} \left(\frac{2\eta\sigma_m}{\sqrt{\pi}} \right)^{2^m-1}. \end{aligned} \quad (29)$$

In the limit of large m we have $\binom{2^{m+1}}{2^m} \sim 4^{2^m}/(\sqrt{\pi}\sqrt{2^m})$. For the success probability it means that it behaves as:

$$p_m(0) \sim \frac{1}{2\sqrt{2^m}} \left(\frac{4}{\sqrt{\pi}} \right)^{2^m} (\eta\sigma_m)^{2^m-1}. \quad (30)$$

Recall that this expression is valid under the constraint that $\eta \cdot \sigma_m \ll 1$. So in particular $\eta\sigma_m \cdot 4/\sqrt{\pi} < 1$ which ensures that the probability remains well-defined. Also note that the notion of scaling is absent from these considerations. Both η and σ_m are fixed parameters here.

3. Impact on the output state

We now focus on the quality of the output binomial state after measuring the $2^m - 1$ ancillary modes. We still consider that the resolution obeys the two conditions mentioned above, namely $\eta \cdot 2^{m-1} \ll 1$ and $\eta \cdot \sigma_m \ll 1$. We can show that in this case the state is actually exactly the correct pure binomial state. We are going to derive this explicitly for the two-mode scenario depicted in Figure 4, which corresponds to the binomial state made of three peaks.

We use the mapping in (23) for two identical squeezed cat states at the input $|\sqrt{2}\sqrt{\pi}, \sigma\rangle + |-\sqrt{2}\sqrt{\pi}, \sigma\rangle$, where $\sigma < 1$. We obtain a two-mode entangled state that reads – with the convention that the first/second ket denotes the upper/lower mode:

$$\begin{aligned} |\psi_1^{\text{bm}}\rangle &= \frac{1}{2} [|0\rangle | -2\sqrt{\pi}, \sigma\rangle + (|2\sqrt{\pi}, \sigma\rangle + | -2\sqrt{\pi}, \sigma\rangle) |0\rangle \\ &\quad + |0\rangle | 2\sqrt{\pi}, \sigma\rangle]. \end{aligned} \quad (31)$$

The upper mode is measured in the \hat{p} quadrature and the outcome 0 is recorded. If we suppose that the resolution satisfies $\eta \cdot 2\sqrt{\pi} = o(1)$ and $\eta \cdot \sigma = o(1)$, then Eq.(27) still holds. With

the notations of this section we have for all $s \in [-\eta, \eta]$ and all $\beta = 0, \pm 2\sqrt{\pi}$:

$${}_p\langle s | \beta, \sigma \rangle \approx \frac{\sqrt{\sigma}}{\pi^{1/4}}. \quad (32)$$

Recall that we assume that the displaced squeezed states are orthogonal to one another. Then the reduced density matrix for the mode being measured ρ_r after tracing over the lower mode reads:

$$\begin{aligned} \rho_r &= \text{Tr}_{\text{low}} [|\psi_1^{\text{bm}}\rangle \langle \psi_1^{\text{bm}}|] \\ &= \frac{1}{4} [2|0, \sigma\rangle \langle 0, \sigma| \\ &\quad + (|2\sqrt{\pi}, \sigma\rangle + |-2\sqrt{\pi}, \sigma\rangle)(\langle 2\sqrt{\pi}, \sigma| + \langle -2\sqrt{\pi}, \sigma|)], \end{aligned} \quad (33)$$

so that the success probability yields, under the assumptions leading to Equation (32):

$$\begin{aligned} p_1(0) &= \int_{-\eta}^{\eta} ds \langle s | \rho_r | s \rangle \\ &= \frac{1}{4} \int_{-\eta}^{\eta} ds [2|{}_p\langle s | 0, \sigma \rangle|^2 + |{}_p\langle s | (|2\sqrt{\pi}, \sigma\rangle + |-2\sqrt{\pi}, \sigma\rangle)|^2] \\ &= \frac{1}{4} \left[2 \cdot 2\eta \frac{\sigma}{\sqrt{\pi}} + 4 \cdot 2\eta \frac{\sigma}{\sqrt{\pi}} \right] \\ &= \frac{3\eta\sigma}{\sqrt{\pi}}. \end{aligned} \quad (34)$$

We can easily check that this is consistent with the general formula derived in Equation (29). We may now compute the output state after obtaining outcome 0 at the measurement. It reads:

$$\rho_1 = \frac{\text{Tr}_{\text{up}} [P_1(0) |\psi_1^{\text{bm}}\rangle \langle \psi_1^{\text{bm}}|]}{p_1(0)}, \quad (35)$$

where $P_1(0) = \int_{-\eta}^{\eta} ds |s\rangle {}_p\langle s|$ is the projector associated with outcome 0 and the upper mode. Then we have:

$$\begin{aligned} \rho_1 &= \frac{1}{p_1(0)} \left(\int_{-\eta}^{\eta} ds {}_p\langle s | \psi_1^{\text{bm}} \rangle \langle \psi_1^{\text{bm}} | s \rangle {}_p \right) \\ &= \frac{1}{6} (|2\sqrt{\pi}, \sigma\rangle + 2|0, \sigma\rangle + |-2\sqrt{\pi}, \sigma\rangle) \\ &\quad \times (\langle 2\sqrt{\pi}, \sigma| + 2\langle 0, \sigma| + \langle -2\sqrt{\pi}, \sigma|), \end{aligned} \quad (36)$$

which is indeed a pure state corresponding to the definition of the first binomial state. This reasoning can be extended by induction to show that binomial states are pure at all orders for a good enough resolution.

Now that we have studied and characterized the binomial states that can be generated using Schrödinger cat states we will describe a protocol that approximately generates the latter using vacuum states.

B. Cat states from coherent states

The protocol for binomial GKP state generation that we have outlined above is based on the use of cat states of the form

$$\frac{1}{\sqrt{2}}(|\alpha\rangle + |-\alpha\rangle). \quad (37)$$

In this section we detail how these states can be generated probabilistically and approximately given a set of elementary

gates and homodyne detection. We use the probabilistic protocol of Ref. [25]. A π -strength cross-Kerr interaction acting on two coherent states of amplitudes $|\alpha_0\rangle$ and $|\beta_0\rangle$ yields

$$e^{i\pi\hat{n}_1\hat{n}_2}|\alpha_0\rangle|\beta_0\rangle = \frac{1}{2}(|\alpha_0\rangle+|-\alpha_0\rangle)|\beta_0\rangle + \frac{1}{2}(|\alpha_0\rangle-|-\alpha_0\rangle)|-\beta_0\rangle. \quad (38)$$

We see from Eq.(38) that if by measuring the second mode one can infer an amplitude of β_0 , then the first mode is projected onto the cat state we are interested in given by Eq.(37), with coherent components of amplitude α_0 . Since the probability density for homodyne detection on the second mode consists of two Gaussians at $\pm\beta_0$ with a very small overlap $\langle-\beta_0|\beta_0\rangle$, this measurement, even with a poor resolution, will be able to discriminate between $|\pm\beta_0\rangle$.

We need hence a viable decomposition of the cross-Kerr operator $e^{i\pi\hat{n}_1\hat{n}_2}$ appearing in Eq.(38) in terms of elementary gates from the universal set. Crucially, the error with which this gate has to be implemented must lie below a fixed threshold, which is related to the desired fidelity on the resulting GKP states. As we will see, this threshold imposes constraints on how the decomposition should be performed.

Several strategies for gate decomposition are possible. In Refs. [28, 29] an alternate technique to *Trotterization* is presented, referred to as *splitting*, or fractal decomposition. This method is particularly suitable when the parameter characteristic of the interaction is small, otherwise very high order decompositions are needed (see condition (44) in Ref. [28]). Inspired by Ref. [26], we use a hybrid ad-hoc strategy that combines these two approaches, and in addition also uses *amplification* preceded by one step of concatenation, in order to first reduce the strength of the Kerr interaction so as to allow splitting. Our decomposition is thereby structured in the following nested steps, that progressively reduce the strength of the interaction applied: (1) One-step concatenation, (2) Amplification, (3) Splitting, and (4) Rescaling. In the following, we describe the decomposition in detail. We use a different order of presentation of the steps listed above, in order to make the presentation clearer.

1. Decomposition of the cross-Kerr interaction

a. Splitting. The operator $\hat{n}_1\hat{n}_2$ defining the cross-Kerr interaction must be split in operators belonging to the set of elementary gates, and that to a precision y . In order to do this, first note that the cross-Kerr operator is given by

$$\begin{aligned} \hat{n}_1\hat{n}_2 &= \frac{1}{2}(\hat{q}^2 + \hat{p}^2 - 1)_1 \otimes \frac{1}{2}(\hat{q}^2 + \hat{p}^2 - 1)_2 \\ &= \frac{1}{4}(\hat{q}_1^2\hat{q}_2^2 + \hat{q}_1^2\hat{p}_2^2 + \hat{p}_1^2\hat{q}_2^2 + \hat{p}_1^2\hat{p}_2^2) - \frac{1}{4}(\hat{q}_1^2 + \hat{p}_1^2) - \frac{1}{4}(\hat{q}_2^2 + \hat{p}_2^2) \\ &\equiv \hat{O}_1 + \hat{O}_2 + \hat{O}_3 + \hat{O}_4 - \frac{1}{4}(\hat{q}_1^2 + \hat{p}_1^2) - \frac{1}{4}(\hat{q}_2^2 + \hat{p}_2^2) \end{aligned} \quad (39)$$

where we have defined $\hat{O}_1 = \hat{q}_1^2\hat{q}_2^2/4$, $\hat{O}_2 = \hat{q}_1^2\hat{p}_2^2/4$, $\hat{O}_3 = \hat{p}_1^2\hat{q}_2^2/4$, $\hat{O}_4 = \hat{p}_1^2\hat{p}_2^2/4$. As we are interested in the cross-Kerr evolution of amplitude π , note that we have

$$e^{i\pi\hat{n}_1\hat{n}_2} = e^{i\pi(\hat{O}_1+\hat{O}_2+\hat{O}_3+\hat{O}_4)}\hat{F}_1^\dagger\hat{F}_2^\dagger. \quad (40)$$

Therefore, we can only focus on the decomposition of the operator $e^{i\pi(\hat{O}_1+\hat{O}_2+\hat{O}_3+\hat{O}_4)}$. Applying twice the second-order

splitting $e^{i\tau(A+B)} = e^{\frac{i\tau}{2}A}e^{i\tau B}e^{\frac{i\tau}{2}A} + O(\tau^3)$ [28] we obtain

$$\begin{aligned} e^{i\tau(\hat{O}_1+\hat{O}_2+\hat{O}_3+\hat{O}_4)} &= \\ e^{i\frac{\tau}{4}\hat{O}_1}e^{i\frac{\tau}{2}\hat{O}_2}e^{i\frac{\tau}{4}\hat{O}_1}e^{i\frac{\tau}{2}\hat{O}_3}e^{i\tau\hat{O}_4}e^{i\frac{\tau}{2}\hat{O}_3}e^{i\frac{\tau}{4}\hat{O}_1}e^{i\frac{\tau}{2}\hat{O}_2}e^{i\frac{\tau}{4}\hat{O}_1} \\ &+ \tau^3 f(\hat{O}_1, \hat{O}_2, \hat{O}_3, \hat{O}_4). \end{aligned} \quad (41)$$

From Eq.(41) we see that, in order to achieve an overall precision y on the cross-Kerr evolution of intensity τ , we have to set $\tau = y^{1/3}$. For this reason, it is important to use small real parameters $\tau < 1$ in the definition of the elementary gates. The exact value of y to be used will be fixed by the desired fidelity between the approximate GKP states resulting from the use of these gates with the standard Gaussian ones, see Sec.VIA. In the following, we use both parameters τ and y to characterize the precision, depending on the convenience.

b. One-step concatenation. Our splitting procedure Eq.(41) results in a gate $e^{i\tau\hat{n}_1\hat{n}_2}$ with intensity $\tau < 1$. Overall however, we need a strength $e^{i\pi\hat{n}_1\hat{n}_2}$ for the cross-Kerr interaction as appearing in Eq.(38). In order to achieve this, one possibility would simply consist in concatenating several times the gate in Eq.(41), i.e. implementing $(e^{i\tau\hat{n}_1\hat{n}_2})^n$. However, reaching high precision is difficult in this way. Therefore, we would rather need a tool to amplify the strength of the cross-Kerr interaction. A recipe for cross-Kerr amplification is provided in Ref. [27]. However, no such amplification is possible that brings us to a π cross-Kerr interaction from an interaction of strength $\tau < 1$. Hence we first use one step concatenation. Namely, we observe that

$$e^{i\pi\hat{n}_1\hat{n}_2} = \left(e^{i\frac{\pi}{2}\hat{n}_1\hat{n}_2}\right)^2, \quad (42)$$

where the resulting cross-Kerr interaction $\pi/2$ is obviously lower than 1. Given that y is the precision with which we are able to implement the gate $\left(e^{i\frac{\pi}{2}\hat{n}_1\hat{n}_2}\right)^2$, then the desired gate $e^{i\pi\hat{n}_1\hat{n}_2}$ is implemented up to precision $2y$.

c. Amplification. In order to amplify the cross-Kerr strength to $\pi/2$, starting from an interaction strength $\tau < 1$, the following identity can be used [27]:

$$e^{i2\gamma\hat{n}_1\hat{n}_2} = \hat{P}'\hat{S}_a e^{i\tau\hat{n}_1\hat{n}_2} \hat{P}\hat{S}_b \hat{P} e^{i\tau\hat{n}_1\hat{n}_2} \hat{S}_a \quad (43)$$

with

$$\begin{aligned} \hat{P} &= e^{-i\frac{\tau}{2}\hat{n}_2} \\ \hat{P}' &= e^{-i(\gamma-\tau)(\hat{n}_1-1/2)+\gamma\hat{n}_2} \\ \hat{S}_i &= e^{-\frac{\theta_i}{2}(\hat{a}_2\hat{a}_2 - \hat{a}_2^\dagger\hat{a}_2^\dagger)} \end{aligned} \quad (44)$$

where $i = a, b$ [42]. Eq.(43) holds provided the following identification can be drawn between the parameters involved:

$$\begin{aligned} \theta_b &= \text{artanh}(-\cos\tau \tanh(2\theta_a)) \\ \gamma &= \arctan(\tan\tau \cosh(2\theta_a)), \end{aligned} \quad (45)$$

and we are interested in the case where

$$\gamma = \frac{\pi}{4}. \quad (46)$$

Eq.(45) can be solved for the squeezing parameters θ_a, θ_b , yielding

$$\begin{aligned} \theta_a &= \pm \frac{1}{2} \text{arcosh}(\cot(\tau)), \\ \theta_b &= -\text{artanh}\left(\cos\left(\sqrt{-\tau^2(\tan^2(\tau)-1)}\right)\right). \end{aligned} \quad (47)$$

A Taylor expansion of the equations above (for the + solution) provides for small τ

$$\begin{aligned}\theta_a &= -\frac{1}{2} \ln \tau + \frac{1}{2} \ln 2, \\ \theta_b &= -2\theta_a,\end{aligned}\quad (48)$$

which establishes a direct relation between the strength of the squeezing parameter to be employed in the amplification step with the interaction strength τ . In turn, we have seen that this parameter is related to the overall precision y by $y = \tau^3$. Therefore, it is possible to estimate the necessary squeezing to amplify the cross-Kerr interaction for a given precision y , namely

$$\theta_a = -\frac{1}{2} \ln y^{\frac{1}{3}} + \frac{1}{2} \ln 2. \quad (49)$$

i.e. (neglecting the constant $\frac{1}{2} \ln 2$)

$$\hat{S}_a = e^{-\frac{\ln s_a}{2}(\hat{a}_2^2 - \hat{a}_1^2)}; \quad \hat{S}_b = e^{-\frac{\ln s_b}{2}(\hat{a}_2^2 - \hat{a}_1^2)} \quad (50)$$

with $s_a = y^{-1/6}$ and $s_b = y^{1/3}$. The squeezing operator is associated with the symplectic action on the quadrature operators:

$$e^{-\frac{\ln s}{2}(\hat{a}^2 - \hat{a}^\dagger^2)} = e^{-i\frac{\ln s}{2}(\hat{q}\hat{p} + \hat{p}\hat{q})} \rightarrow \begin{pmatrix} \hat{q}' \\ \hat{p}' \end{pmatrix} = \begin{pmatrix} s & 0 \\ 0 & 1/s \end{pmatrix} \begin{pmatrix} \hat{q} \\ \hat{p} \end{pmatrix}, \quad (51)$$

and

$$\sigma_{\text{dB}}^2 = -10 \log_{10} \left(\frac{\sigma^2}{\Delta_0^2} \right) = -10 \log_{10} (s^2). \quad (52)$$

As a consequence, we can estimate the total amount of needed squeezing as

$$\sigma_{\text{dB},a}^2 = -10 \log_{10} \left(\frac{\sigma^2}{\Delta_0^2} \right) = -10 \log_{10} (y^{\frac{1}{3}}), \quad (53)$$

$$\sigma_{\text{dB},b}^2 = -10 \log_{10} \left(\frac{\sigma^2}{\Delta_0^2} \right) = -10 \log_{10} (y^{\frac{2}{3}}) = 2\sigma_{\text{dB},a}^2,$$

i.e. for instance $\sigma_{\text{dB},a}^2 = 10$ dB and $\sigma_{\text{dB},b}^2 = 20$ dB for $y = 10^{-3}$ and $\sigma_{\text{dB},a}^2 = 3.3$ dB and $\sigma_{\text{dB},b}^2 = 6.7$ dB for $y = 10^{-1}$.

d. Rescaling. We now have to decompose the factors appearing in Eq.(41). From Eq.(5) of Ref. [26] we have [43]

$$\hat{p}_1^2 \hat{p}_2^2 = -\frac{1}{9} [\hat{p}_2^3, [\hat{p}_1^3, \hat{q}_1 \hat{q}_2]]. \quad (54)$$

The evolution stemming from the operator $\hat{q}_1 \hat{q}_2$ belongs to our set of gates, while those corresponding to \hat{p}_2^3 and \hat{p}_1^3 can be obtained by Fourier-transforming the cubic phase gate also in the set, namely $\hat{p}^3 = \hat{F} \hat{q}^3 \hat{F}^\dagger$. The other terms of Eq.(39) can be obtained by Fourier transforming on one or two modes, e.g.

$$e^{\frac{i\tau \hat{q}_1^2 \hat{q}_2^2}{4}} = \hat{F}_1^\dagger \hat{F}_2^\dagger e^{\frac{i\tau \hat{p}_1^2 \hat{p}_2^2}{4}} \hat{F}_1 \hat{F}_2. \quad (55)$$

Therefore, it is only necessary to further decompose the operator in Eq.(54), namely the evolution $e^{\frac{i\tau \hat{p}_1^2 \hat{p}_2^2}{4}} = e^{-\frac{i\tau [\hat{p}_2^3, [\hat{p}_1^3, \hat{q}_1 \hat{q}_2]]}{36}}$.

Rescaling can be carried out as done in the supplementary material of Ref. [26]. In Appendix A we derive the rescaling

equations relevant to our purposes, in analogy to the derivation presented in Ref. [26]. We obtain

$$\begin{aligned}e^{i\tau[\hat{B}, [\hat{C}, \hat{A}]]} &= \left(e^{i\hat{B} \frac{\tau^{1/3}}{k}} \left(e^{i\hat{A} \frac{\tau^{1/3}}{kl}} e^{i\hat{C} \frac{\tau^{1/3}}{kl}} e^{-i\hat{A} \frac{\tau^{1/3}}{kl}} e^{-i\hat{C} \frac{\tau^{1/3}}{kl}} \right)^{l^2} \right. \\ &\quad \left. e^{-i\hat{B} \frac{\tau^{1/3}}{k}} \left(e^{-i\hat{A} \frac{\tau^{1/3}}{kl}} e^{-i\hat{C} \frac{\tau^{1/3}}{kl}} e^{i\hat{A} \frac{\tau^{1/3}}{kl}} e^{i\hat{C} \frac{\tau^{1/3}}{kl}} \right)^{l^2} \right)^{k^3} \\ &\quad + O\left(\frac{\tau^{4/3}}{k}\right) + O\left(\frac{\tau}{l}\right),\end{aligned}\quad (56)$$

which we can now use (upon a further rescaling $\tau \rightarrow -\tau/36$) with the following identification of the operators in Eq.(54): $\hat{A} = \hat{q}_1 \hat{q}_2$ and $\hat{B} = \hat{p}_2^3$ and $\hat{C} = \hat{p}_1^3$. Since in Eq.(41) there appear 9 operators that require a decomposition of the kind in Eq.(56), in order to provide a more conservative estimate we require that each factor is implemented up to a precision $\tau^3/9$. Therefore we must require the identifications $\tau^{4/3}/(36^{4/3}k) \sim \tau^3/9$ and $\tau/(36l) \sim \tau^3/9$, which implies

$$\begin{aligned}k &\sim 9^{-\frac{1}{3}} 4^{-\frac{4}{3}} \tau^{-\frac{5}{3}} = 9^{-\frac{1}{3}} 4^{-\frac{4}{3}} y^{-\frac{5}{9}} \\ l &\sim \tau^{-2}/4 = y^{-\frac{2}{3}}/4.\end{aligned}\quad (57)$$

We stress again that the final precision $y = \tau^3$ on the cat state generation impacts the quality of the binomial GKP states that are generated with this protocol. More precisely, since a binomial state of order m requires 2^m cat states, the error y is amplified accordingly: for a given m , the distance between the approximate GKP states generated through this procedure and the binomial states is upper bounded by $2^m y$. We indicate the approximate binomial GKP states by $|\bar{0}_m\rangle$. A summary of the fidelities between different GKP states is provided in Table 6.

To summarize, we have provided a decomposition of the cross-Kerr interaction $e^{i\pi \hat{n}_1 \hat{n}_2}$ in gates of the form $e^{ib\hat{q}_1 \hat{q}_2}$, $e^{ic\hat{q}^3}$, $e^{ig(\hat{q}\hat{p} + \hat{p}\hat{q})}$, \hat{F} . In Appendix B we provide an estimate of the scaling of the required number of gates in order to achieve a precision of y , which results in $N \propto y^{-3}$. This results in particular in a thousand elementary gates for a required precision of 0.1 in the cross-Kerr gate implementation.

What we further have to do is to provide a decomposition of the squeezing gate $e^{ig(\hat{q}\hat{p} + \hat{p}\hat{q})}$ in terms of the elementary gates of Eqs.(7) and (8). Also, in the procedure outlined above for the GKP synthesis from cat states a beamsplitter appears. Therefore we must also decompose this transformation into elementary gates. This is the goal of the next subsection.

2. Decomposition of beam splitters and squeezers

In order to cast the gates used for the cross-Kerr evolution in the form admitted by the set A_1 we have to provide an expression of the squeezing operator and of the beamsplitter in terms of \hat{q} -diagonal gates and Fourier transforms. In contrast to the decomposition of the previous subsection, these can be provided exactly. We provide the detailed calculation in Appendix C. The result is the following: the squeezing operator is decomposed onto

$$e^{-i\frac{\ln s}{2}(\hat{q}\hat{p} + \hat{p}\hat{q})} = \hat{F} e^{\frac{is\hat{q}^2}{2}} \hat{F} e^{\frac{i\hat{q}^2}{2s}} \hat{F} e^{\frac{is\hat{q}^2}{2}}, \quad (58)$$

while the beam splitter operator decomposes as

$$\hat{F}O(\hat{q})FO(\hat{q})FO(\hat{q}) \quad (59)$$

with $O(q) = e^{i\frac{1}{2\sqrt{2}}(\hat{q}_1^2 - \hat{q}_2^2 + \hat{q}_1\hat{q}_2)}$. Note that in turn $O(\hat{q})$ can be trivially decomposed in shear and \hat{C}_Z gates. Now all the gates necessary to implement an approximate GKP state have been decomposed onto gates of the elementary set Eqs.(7) and (8).

Approximate GKP	\rightarrow	Binomial GKP	\rightarrow	Gaussian GKP
$ \tilde{0}_m\rangle$	$2^m y$	$ 0_m\rangle$	ζ_m	$ 0_G\rangle$

FIG. 6: Summary of the definitions for the different fidelities between GKP states addressed in this paper. The overall distance between $|\tilde{0}_m\rangle$ and $|0_G\rangle$ is $\varepsilon_m = \zeta_m + 2^m y$. Also note that the respective encoded data qubits share the same trace distances, due to the fact that encoding consists of a unitary operation.

V. Noise in CV and fault tolerance

Fault tolerance in CV is an issue that must be addressed specifically. In this section we show that the universal model defined in III A can be made fault tolerant.

In CV, the natural basis for quantum channels consists of all possible displacement operators. Formally, a general noise model \mathcal{E} on an arbitrary input state $\hat{\rho}$ can be expanded in terms of shifts acting on $\hat{\rho}$, according to the following expression:

$$\mathcal{E}(\hat{\rho}) = \int du dv du' dv' C(u, v, u', v') e^{-iu\hat{p}} e^{-iv\hat{q}} \hat{\rho} e^{iv'\hat{q}} e^{iu'\hat{p}}. \quad (60)$$

Therefore an error correcting procedure in CV applies to arbitrary noise models if it allows one to correct for arbitrary displacement errors (similar to qubits where an arbitrary error can be corrected based on Pauli-error correction). This feature is enabled by the GKP encoding [16] using an additional source of ancillary GKP $|0_G\rangle$ states, where as we have already noted the notation $|0_G\rangle$ indicates that the ancillary GKP states employed are the Gaussian ones, i.e. enveloped by a Gaussian and correspondingly associated with a finite squeezing degree. The specific circuit for error-correction is shown in Fig. 7.

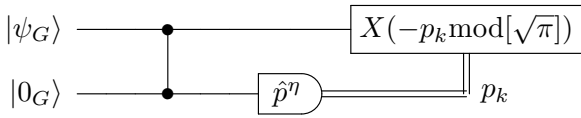


FIG. 7: Procedure to correct for errors in the \hat{q} quadrature. $|\psi\rangle$ is the data qubit and $|0_G\rangle$ is a Gaussian GKP state. After measurement on the second mode the result p_k is used to shift the first mode back.

The noise reduction (i.e. error-correction in the CV sense) works if the measurement on the ancillary mode yields the correct $\sqrt{\pi}$ -long interval on the real axis. The displacement error acting on the data qubit in one of the quadratures is then replaced by the independent error coming from the

fresh ancillary GKP state. Repeating the procedure after a Fourier transform ensures that the displacement errors in both quadratures are replaced. To summarize, this probabilistic procedure ensures that the CV noise remains controlled and determined by the noise linked to the supply of GKP states. The success probability itself is determined by how likely the noise is to displace the state by more than $\sqrt{\pi}/2$.

An important step was taken in [17], where the authors combined this noise reduction procedure with an additional layer of qubit error-correcting code at the logical encoding level. They showed that if the procedure fails – that is the measured displacement error was larger than $\sqrt{\pi}/2$ – the controlled-displacement actually corresponds to a bit flip at the GKP encoding level. Then one can use a standard qubit error-correcting code to address this bit flip error. This ensures that the failure probability of the procedure, as soon as it is lower than the threshold associated with the qubit error-correcting code, can be made arbitrarily small, thus enabling fault tolerance for a CV hardware. Note that the squeezing level required in order to fulfill the threshold condition according to the procedure described above can be lowered by utilizing a more refined error-correction scheme [30]. The latter exploits a priori information stemming from the Gaussian distribution in each GKP peak, rather than only using binary information corresponding to the measured displacement being ‘inside’ or ‘outside’ the above mentioned $\sqrt{\pi}$ -long interval. This method also allows for the reduction of the number of the concatenation steps in a full error-correcting procedure [31]. For the purpose of keeping our discussion less technical, however, we will refer to the original error-correction scheme of Ref. [17] in order to derive bounds on the squeezing level as well as other approximations levels to be used in our model.

In practice then, the success probability is determined by how likely the noise is to displace the state by more than $\sqrt{\pi}/2$. There may be numerous origins for this CV noise: usually not only the “data qubit” will be noisy, but the ancillary one and the measurement (e.g. finite resolution) will also. Crucially the characteristics of the noise do not really matter. The only relevant questions are: what is the probability that all these errors put together yield a displacement larger than $\sqrt{\pi}/2$? Is it possible to make this probability lower than the threshold of some qubit error-correcting code ε_{th} ? Mathematically, we aim to analyse and upper bound the following probability:

$$\Pr\left(|p| > \frac{\sqrt{\pi}}{2}\right), \quad (61)$$

where p is the displacement error measured in the protocol shown in Fig. 7. However this probability may turn out to be too difficult to compute. We show in the following how to reduce this problem to a much simpler one only involving Gaussian functions.

We are going to assume GKP encoding as explained above. The data qubit is however encoded in the approximate GKP states basis obtained with the procedure outlined in Section IV. We denote the corresponding density matrix with $\tilde{\rho}_m$. When noise enters the picture the output state ρ can be a mixed state. We characterize the noise model by a parameter ε which upper bounds the distance:

$$d(\rho, \tilde{\rho}_m) \equiv \frac{1}{2} \|\rho - \tilde{\rho}_m\| < \varepsilon \quad (62)$$

where $\|\cdot\|$ indicates the standard trace norm. Similarly we can upper bound the distance between the approximate GKP

states and the standard Gaussian GKP states $|0/1_G\rangle$. Recall that it is determined by two contributions: ζ_m coming from the imperfect fidelity between the binomial states and the Gaussian GKP states – see Table 5 Table 6 and Eq.(19); and $2^m y$ because of the approximate procedure used to generate Schrödinger cat states and thus approximate GKP states, stemming from finite precision gates – see the discussion following Eq.(57). Sticking with the density matrix formalism for consistency, we denote as ρ_G the closest Gaussian GKP-encoded state to the corresponding approximate GKP-encoded state $\tilde{\rho}_m$:

$$d(\tilde{\rho}_m, \rho_G) < \varepsilon_m, \quad (63)$$

where $\varepsilon_m = \zeta_m + 2^m y$.

Suppose now that one wishes to reduce the noise of a state ρ using the procedure described in Fig. 7. There, the input state is $\rho_G |0_G\rangle \langle 0_G|$, where the tensor product is implicit. In our scheme, the input state is replaced by $\rho |\tilde{0}_m\rangle \langle \tilde{0}_m|$, where $|\tilde{0}_m\rangle$ is the logical 0 state encoded in the approximate GKP basis. We focus first on the trace distance for the joint state after the C_Z gate represented in Fig. 7. For a perfect, unitary C_Z gate and using properties of the trace norm we have:

$$\begin{aligned} d(C_Z \rho |\tilde{0}_m\rangle \langle \tilde{0}_m| C_Z^\dagger, C_Z \rho_G |0_G\rangle \langle 0_G| C_Z^\dagger) \\ &= d(\rho |\tilde{0}_m\rangle \langle \tilde{0}_m|, \rho_G |0_G\rangle \langle 0_G|) \\ &\leq d(\rho |\tilde{0}_m\rangle \langle \tilde{0}_m|, \tilde{\rho}_m |\tilde{0}_m\rangle \langle \tilde{0}_m|) \\ &\quad + d(\tilde{\rho}_m |\tilde{0}_m\rangle \langle \tilde{0}_m|, \rho_G |\tilde{0}_m\rangle \langle \tilde{0}_m|) \\ &\quad + d(\rho_G |\tilde{0}_m\rangle \langle \tilde{0}_m|, \rho_G |0_G\rangle \langle 0_G|) \\ &< \varepsilon + \varepsilon_m + \varepsilon_m. \end{aligned} \quad (64)$$

In other words, the statistical distance for the noise reduction protocol using approximate GKP states as ancillary qubits compared to using Gaussian GKP states is upper bounded by $\varepsilon + 2\varepsilon_m$. Hence the possible deviations of the measurement results are also upper bounded by $\varepsilon + 2\varepsilon_m$.

We now define p (p_G) as the measured displacements in the (Gaussian) protocol. Eq. (64) implies that $|p - p_G| < \varepsilon + 2\varepsilon_m$. Let us consider now the failure probability that we wish to upper bound, that is

$$\begin{aligned} P_{\text{fail}} &= \Pr(|p| > \sqrt{\pi}) = \Pr\left(|p - p_G + p_G| > \frac{\sqrt{\pi}}{2}\right) \\ &\leq \Pr\left(|p_G| + |p - p_G| > \frac{\sqrt{\pi}}{2}\right) \\ &\leq \Pr\left(|p_G| > \frac{\sqrt{\pi}}{2} - |p - p_G|\right) \\ &\leq \Pr\left(|p_G| > \frac{\sqrt{\pi}}{2} - (\varepsilon + 2\varepsilon_m)\right). \end{aligned} \quad (65)$$

In other words, if we aim to upper bound the probability that our error-correction protocol fails – and show that it can be made lower than some threshold probability ε_{th} – we simply have to consider the Gaussian protocol using $\sqrt{\pi}/2 - (\varepsilon + 2\varepsilon_m)$ as a bound rather than $\sqrt{\pi}/2$.

Recall finally that the protocol actually needs to be repeated after a Fourier transform to cover for the noise in both quadratures. The protocol is successful if both rounds are, i.e. the total failure probability can be expressed as

$$1 - P_{\text{succ}1} P_{\text{succ}2} = 1 - (1 - P_{\text{fail}1})(1 - P_{\text{fail}2}), \quad (66)$$

where 1 and 2 refer to error-correction rounds on the two respective quadratures. For real σ and δ we denote $\chi(\sigma, \delta) = \Pr(|p_G(\sigma)| > \sqrt{\pi}/2 - \delta)$, where we stress that p_G actually depends on the squeezing σ of the Gaussian GKP states. A given noise model corresponds to non-vanishing values for the distances ε and ε_m . Then, combining Eq.(65) and (66), the fault tolerance condition amounts to finding a squeezing parameter σ_{th} such that the following bound on the total failure probability holds:

$$1 - (1 - \chi(\sigma_{\text{th}}, \varepsilon_q + 2\varepsilon_m))(1 - \chi(\sigma_{\text{th}}, \varepsilon_p + 2\varepsilon_m)) < \varepsilon_{\text{th}}. \quad (67)$$

Note that in principle the Fourier transform in between the two rounds of noise reduction may disturb the system and thus yield a different upper bound for the trace distance, hence the notation $\varepsilon_{1,2}$ – e.g. the Measurement Based implementation of the Fourier transform (see e.g. the Supplementary Information of Ref. [18] for a detailed discussion).

Thus we have shown how to reduce an arbitrary noise model to simply considering Gaussian GKP states with slightly modified thresholds. This allows one to easily compute the relevant probabilities since they consist in integrating tails of Gaussian functions.

VI. Consequences for the CV gates

In this section we determine the conditions that fault-tolerance requirements impose on the gate parameters defined in section III Eqs.(7) and (10). They also depend on the precision of the gate decomposition that we have derived in the previous sections.

A. Universal computational model

The gates belonging to the universal computational model that we have introduced in Sec. III A are assumed to be perfectly implemented. Thus no active error-correction is required. However, the results detailed in Section V pave the way for fault tolerance: whatever noise model one has to deal with, it can be plugged in our computational model to be translated into specific requirements for the gate parameters and still allow for error correction.

Here, we find instructive to discuss the case as in the abstract definition of our model, where the gates belonging to the computational model are assumed to be perfectly implemented. It corresponds to setting $\varepsilon_q = \varepsilon_p = 0$ and no active error-correction is required. However using approximate GKP states for logical information encoding yields an intrinsic error probability. Following the analysis performed in [16], this probability can be linked to the integrals of Gaussian functions, i.e. to the error function. For a Gaussian GKP state of symmetric squeezing parameter σ it simply reads $\text{erf}(\sqrt{\pi}/2\sigma)$, where erf denotes the error function. In our case this probability also depends on the ε_m defined in Eq.(63), as well as on the gate parameters required for universal quantum computing. Namely we have:

$$P_{\text{succ}}(m, y) = \text{erf}\left(\frac{\frac{\sqrt{\pi}}{2} - \varepsilon_m}{\sigma}\right), \quad (68)$$

where m and σ are related according to the discussion in Sec. IV, and where in particular ε_m depends on the precision y .

We consider the experimentally easiest case where $m = 1$, so $\varepsilon_1 = \zeta_1 + 2y$. Given the analysis performed in Sec. IV, the corresponding approximate GKP states can be compared to Gaussian GKP states with a squeezing parameter of 5 dB. The associated fidelity shown in Table 5 can be used to estimate ζ_1 :

$$\zeta_1 \leq \sqrt{1 - 0.9976^2} \approx 0.069. \quad (69)$$

In order to compute the corresponding gate parameters, we plot in Fig. 8 the success probability P_{succ} as a function of the errors y in the implementation of the cross-Kerr interaction discussed in Sec. IV. It reads:

$$P_{\text{succ}}(y) = \text{erf}\left(\frac{\frac{\sqrt{\pi}}{2} - \zeta_1 - 2y}{\sigma}\right). \quad (70)$$

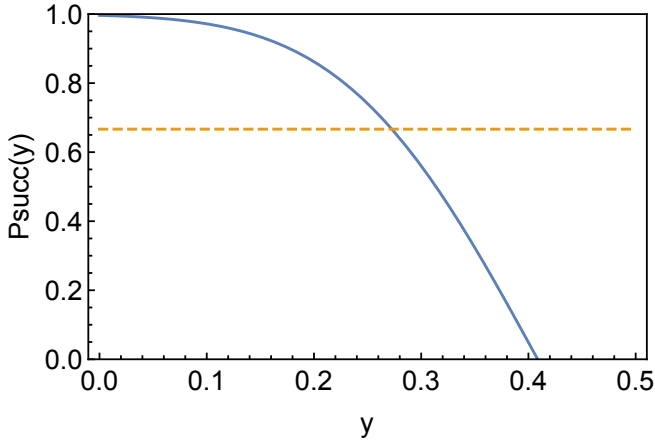


FIG. 8: Success probability P_{succ} in Eq.(70) as a function of y (solid line). As a guide for the eye, the reference level $2/3$ is also plotted (dashed line).

To a value of the gate precision of $y = 0.1$ corresponds a success probability of approximately 0.97. Therefore in the following we will use this value to derive the corresponding gate parameters and understand the experimental consequences.

Based on this requirement of $y = 0.1$ and $m = 1$, we can now compute the gate parameters corresponding to the gate set A_1 defined in Sec. III A, Eqs.(7) and (8). As drawn from the previous sections, using in particular Eqs.(56) and (58) we obtain the numerical values summarized in table Tab.9. Together with the gates required to implement the beam splitter appearing in Eq.(59), this completes the set of gates that defines our model.

B. Subuniversal models

In this section we provide a proof of classical computational hardness of exact sampling in the worst-case scenario for both subuniversal models introduced in Sec.III B. First we focus on the circuit represented in Fig.2, and argue that its hardness directly follows as a consequence of the universality of the

Evolution	GKP generation step	Parameters
Displacement	Coherent state initialization	$d \simeq 5.6$
Shearing	Squeezing in amplification and squeezing of the cat	$s_1 \simeq 0.23$; $s_2 \simeq 0.34$ $s_3 \simeq 0.73$; $s_4 \simeq 1.1$
Entanglement	Beamsplitter	$\tilde{b}_1 \simeq 0.35$
	Cross-Kerr decomposition	$\tilde{b}_2 \simeq 0.74$
Cubic	Cross-Kerr decomposition	$c_1 \simeq 0.74$; $c_2 \simeq 0.86$

FIG. 9: Summary of the parameters for the definition of the gates of the universal model Eqs.(7) and (8), based on a precision of $y = 0.1$ and $m = 1$.

model of computation that we have addressed in Sec.VI A. Then, we turn to CVIQP (Fig.3), and refine the proof that was provided in Ref. [18] by dropping the requirement of input GKP states. To achieve this goal, we use similar arguments to those that allowed us to claim fault-tolerance in the probabilistic universal model that we have presented. As we shall see, the required constraints are tighter for the latter model.

1. CV random circuit sampling

The first circuit that we address is represented in Fig.2, corresponding to picking gates randomly from the sets that define the probabilistic and universal computational model discussed in the previous section VI A. For the case of exact sampling, a very standard proof of classical hardness can be provided [18, 32–34]. In general, if a subuniversal computational model of quantum computation becomes universal when post-selecting on a subset of the outputs – i.e. contains the class PostBQP, then information-theoretic arguments allow one to conclude that efficient classical simulation of this subuniversal model is impossible. These arguments are based on widely-held conjectures of classical complexity theory, like the so-called Polynomial Hierarchy not collapsing. Hence the main point that we have to show is that post-selection makes the circuit of Fig.2 as powerful as PostBQP.

This statement directly follows from the universality of the model presented in VI A. As we have shown in Sec.IV, the gates in Eq.(7) allow for the probabilistic generation of approximate GKP states with success probability given by Eq.(29). Crucially, the fact that the success probability is exponentially low in the number of approximate GKP states that need to be produced does not hinder this result [35]. Therefore, any quantum circuit can be run probabilistically using elements drawn only from the family of circuits of Fig.2. Then post-selecting on successfully passing these probabilistic events yields the correct computation. Furthermore, one can also post-select on an additional subset of the outputs. It means that universal and post-selected quantum computations – i.e. PostBQP – can be performed using circuits of the type described in Fig.2.

We also stress that post-selection should be regarded as a mathematical trick for the proof of hardness, and that experimentally probing the model under consideration would just consist in sampling from an architecture belonging to the family depicted in Fig.2, with no actual need for practical post-selection on measurement outcomes, nor for actual

generation of GKP states.

2. CV Instantaneous Quantum Computing with input squeezed states is hard

The second circuit family we address is sketched in Fig.3. In order to show that the model CVIQP is hard to sample classically, we build on the proof presented in [18], that was established for an analogous model, but with Gaussian GKP states available at the input. The squeezing parameter of those GKP states, furthermore, was required to scale logarithmically with the circuit size, namely we had

$$\sigma \propto \log n \quad (71)$$

where σ in dB characterizes the widths of the Gaussian describing the GKP states wavefunction and n is the number of modes. Just like for the model addressed in Sec.VIB1, the main structure of reasoning to claim computational hardness was based on showing that the class defined as PostCVIQP, i.e. CVIQP with the additional resource of post-selection, is as powerful as PostBQP. In other words, that PostCVIQP is a universal and fault tolerant model of QC – supplemented with post-selection.

In order to obtain universality and fault-tolerance in the post-selected model (i.e. to show that it is as powerful as PostBQP), we first show that the condition (71) is actually unnecessary for the hardness statement of Ref.[18] to hold, and that a constant σ is sufficient to prove the hardness of the circuit. Furthermore, note that the GKP state generation can be subsumed in the circuit model definition when this is augmented with post-selection, similarly as we did in VIB1. Then, we analyze the bound on the input squeezing imposed by the fault-tolerance requirement of the model with post-selection.

The probability of a successful post-selection only makes sense if it is not worse than exponentially low, which in particular is guaranteed by the scaling law for the squeezing parameter derived in [18]. However, the post-selection happens at a logical, encoding level so it actually corresponds to several physical measurement outcomes recombined according to the error-correcting code. Each of these outcomes is noisy because of the CV nature of the quantum states, which can be understood as having imperfect, non-orthogonal qubits. However, the threshold theorem states that the probability of reaching a wrong conclusion at the encoding level can be made exponentially low since the physical noise can be mapped to a qubit error following the procedure described in the previous section.

More specifically, this mapping is ensured by the use of GKP states, and by associating the measurement outcomes of the homodyne detection in given intervals to either 0 or 1 at the logical level. For a symmetric Gaussian noise, an upper bound as a function of the squeezing can be found in [16] with additional approximations. Therefore, the scaling condition in Eq.(71) was actually unnecessary.

Now, recall that the proof of hardness for CVIQP circuits holds if we can make sure that PostCVIQP circuits are able to realize universal quantum computations. However, since the Fourier transform does not belong to the computational model defined by CVIQP circuits, it can only be implemented in PostCVIQP using a measurement-based approach as shown in Fig.11. This approach unfortunately introduces additional

noise, which implies that we have to rely on quantum error-correction for CV quantum computation as discussed in Section V.

The Fourier transform can be implemented in a single, post-selected, teleportation step. The squeezing parameter σ characterizing the squeezed vacuum state is added to the variance of the momentum quadrature of the state being teleported. Based on the analyses developed in Section V and Ref. [17] and neglecting the effects of finite resolution, a sufficient condition to achieve fault tolerance can be derived, similar to the one in Eq. (67), and reads:

$$1 - \left(1 - \chi(\sqrt{2}\sigma, 2\varepsilon_m)\right) \left(1 - \chi(\sqrt{5}\sigma, 2\varepsilon_m)\right) < \varepsilon_{\text{th}}, \quad (72)$$

for a given qubit error-correcting code of threshold probability ε_{th} .

We chose the lowest value of m compatible with Eq. (72). For a threshold probability $\varepsilon_{\text{th}} = 10^{-6}$ we find that $m = 6$, which corresponds to a squeezing of 19 dB according to Eq. (16), is the minimal amount of squeezing that satisfies Eq. (72). It yields an upper bound on $\varepsilon_6 \approx 0.05$. Recall that $\varepsilon_6 = 2^6 y + \zeta_6$. Using Eq. (19) we have $\zeta_6 \approx 3 \cdot 10^{-3}$ so we get an upper bound for the error rate in the Schrödinger cat states generation of

$$y \leq 10^{-3}. \quad (73)$$

This value constitutes a much stronger requirement than the value of 10^{-1} found in Sec. VIA when discussing the model for universal quantum computing. It stems from the fact that the set of gates in CVIQP circuits does not include the Fourier transform, which must be implemented in a measurement-based fashion entailing an additional error due to finite squeezing in the ancillary squeezed state. Analogous to what we found for the universal model in Table 9, this value of precision allows for the derivation of corresponding gate parameters for the definition of the CVIQP model of Eq.(10). These parameters are shown in Table 10.

Evolution	GKP generation step	Parameters
Displacement	Coherent state initialization	$\tilde{d} \simeq 142$
Shearing	Squeezing in amplification	$\tilde{s}_1 \simeq 0.05; \tilde{s}_2 \simeq 0.16$ $\tilde{s}_3 \simeq 1.6; \tilde{s}_4 \simeq 5$
	and squeezing of the cat	$\tilde{s}_5 \simeq 0.28; \tilde{s}_6 \simeq 0.89$
Entanglement	Beamsplitter	$\tilde{b}_1 \simeq 0.35$
	Cross-Kerr decomposition	$\tilde{b}_2 \simeq 1.6 \cdot 10^{-3}$
Cubic	Cross-Kerr decomposition	$\tilde{c}_1 \simeq 1.6 \cdot 10^{-3}$
		$\tilde{c}_2 \simeq 0.86$

FIG. 10: Summary of the parameters for the definition of the gates of the CVIQP model, based on a precision of $y = 10^{-3}$ and $m = 6$. Note that some of the shearing gate parameters above appear in a ratio of 10 or 100. Hence, in principle the gates with strength s_3 and s_4 could be obtained by repeating those with s_1 and s_2 several times.

In conclusion to this section on subuniversal models, we stress that neither for the CV random circuit sampling model discussed in Sec.VIB1, nor for CVIQP actual generation of GKP states is needed in practice: the statement on computational hardness holds for sampling from the output probability distributions of the circuits in Fig.2 and Fig.3, respectively.

In contrast to the universal model, GKP generation and encoding was only used as a conceptual intermediate step for the proof of hardness.

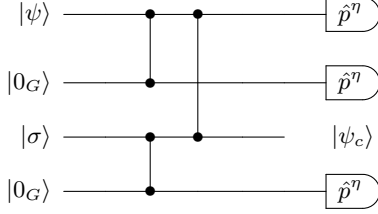


FIG. 11: Circuit implementation of an error-corrected Fourier transform based on the resources available in the CVIQP model, where $|\psi_c\rangle$ denotes the output corrected state.

VII. Conclusions

In summary, we have derived what is to our knowledge the first computational model in CV based on vacuum states, and we have shown that a finite set of gates and homodyne detection are sufficient to achieve probabilistic universal QC and fault tolerance. This model can be adapted to yield sampling problems which are hard to sample for classical computers unless the polynomial hierarchy collapses. These consist of a CV random circuit sampling model with the same structure as for universal computations, and a model analogous to IQP for qubits, based on momentum squeezed vacuum states.

Regarding fault-tolerance considerations, in the universal model the gates are implemented perfectly, and no active correction is required. However the intrinsic noise inherent to approximate GKP states can be linked to the parameters of the gates defining our model, allowing to determine the value of the gate parameters to use. Consistently with that gate parameters, GKP states generated from two Schrödinger cat states can be used, which is experimentally not too demanding. The hardness proof for the CV random circuit model, which is directly drawn on the basis of the universal model, relies on similar considerations.

On the other hand, for the CVIQP model, more stringent requirements on fault-tolerance are imposed by the fact that the Fourier transform does not belong to the gate set. Correspondingly, stronger constraints on the squeezing parameter and gate precision arise.

We believe our work opens up new perspectives. Concerning the universal model, several aspects can be further optimized, from the gate decomposition [28] of the cross-Kerr implementation to the error-correcting procedure [36]. A further way to drastically reduce the number of gates necessary for the implementation of the cross-Kerr interaction could be to include in the elementary gates set a quartic Hamiltonian e^{iq^4} [37].

Furthermore, it would be interesting to study specific implementation of the gates that compose our model. For instance, in Ref. [38] a protocol was given, allowing for the implementation of polynomial approximation of arbitrary-order operations diagonal in the \hat{q} quadrature (including non-Gaussian operations), with the use of ancillary photon-subtracted squeezed states. Merging the two approaches,

upon proper considerations on error-probability and fault-tolerance specific to the gate implementation considered, would result in probabilistic fault-tolerant universal QC from photon subtracted squeezed states and Gaussian operations as building blocks. As for the sampling models considered, it would be desirable to extend the hardness proof to the average case, and to the approximate sampling case.

VIII. Acknowledgements

We acknowledge Nicolas Menicucci and Rafael Alexander for useful discussions. This work was supported by the ANR COMB project, grant ANR-13-BS04-0014 of the French Agence Nationale de la Recherche.

A. Nested commutators used for the rescaling step

The starting point is

$$e^{t^2[\hat{B}, \hat{A}]} = e^{it\hat{B}} e^{it\hat{A}} e^{-it\hat{B}} e^{-it\hat{A}} + O(t^3, \hat{A}, \hat{B}). \quad (\text{A1})$$

Now using the identity $e^{t^2[\hat{B}, \hat{A}]} = e^{(\frac{t}{n})^2[\hat{B}, \hat{A}]n^2}$ and using Eq.(A1) with $t \rightarrow t/n$ we obtain

$$\begin{aligned} e^{t^2[\hat{B}, \hat{A}]} &= \left(e^{i\frac{t}{n}\hat{B}} e^{i\frac{t}{n}\hat{A}} e^{-i\frac{t}{n}\hat{B}} e^{-i\frac{t}{n}\hat{A}} + O\left(\frac{t^3}{n^3}, \hat{A}, \hat{B}\right) \right)^{n^2} \\ &= \left(e^{i\frac{t}{n}\hat{B}} e^{i\frac{t}{n}\hat{A}} e^{-i\frac{t}{n}\hat{B}} e^{-i\frac{t}{n}\hat{A}} \right)^{n^2} + O\left(\frac{t^3}{n}, \hat{A}, \hat{B}\right). \end{aligned} \quad (\text{A2})$$

The standard equation for the nested commutator is then derived by replacing in Eq.(A1) $it\hat{A} \rightarrow t^2[\hat{B}, \hat{A}]$. We then obtain

$$e^{it^3[\hat{B}, [\hat{B}, \hat{A}]]} = e^{it\hat{B}} e^{t^2[\hat{B}, \hat{A}]} e^{-it\hat{B}} e^{-t^2[\hat{B}, \hat{A}]} + O(t^4, \hat{A}, \hat{B}). \quad (\text{A3})$$

Similarly as done before, we now use the identity $e^{it^3[\hat{B}, [\hat{B}, \hat{A}]]} = e^{i(\frac{t}{m})^3[\hat{B}, [\hat{B}, \hat{A}]]m^3}$ so that we obtain

$$\begin{aligned} e^{it^3[\hat{B}, [\hat{B}, \hat{A}]]} &= \left(e^{i\frac{t}{m}\hat{B}} e^{i(\frac{t}{m})^2[\hat{B}, \hat{A}]} e^{-i\frac{t}{m}\hat{B}} e^{-i(\frac{t}{m})^2[\hat{B}, \hat{A}]} \right)^{m^3} \\ &\quad + O\left(\frac{t^4}{m}, \hat{A}, \hat{B}\right). \end{aligned} \quad (\text{A4})$$

Now finally we replace Eq.(A2) in Eq.(A4), but with $t \rightarrow t/m$, i.e. we use $e^{(\frac{t}{m})^2[\hat{B}, \hat{A}]} = e^{(\frac{t}{ml})^2[\hat{B}, \hat{A}]l^2}$, yielding

$$\begin{aligned} e^{it^3[\hat{B}, [\hat{B}, \hat{A}]]} &= \left(e^{i\hat{B}\frac{t}{m}} \left(e^{i\hat{A}\frac{t}{ml}} e^{i\hat{B}\frac{t}{ml}} e^{-i\hat{A}\frac{t}{ml}} e^{-i\hat{B}\frac{t}{ml}} \right)^{l^2} \right. \\ &\quad \left. e^{-i\hat{B}\frac{t}{m}} \left(e^{-i\hat{A}\frac{t}{ml}} e^{-i\hat{B}\frac{t}{ml}} e^{i\hat{A}\frac{t}{ml}} e^{i\hat{B}\frac{t}{ml}} \right)^{l^2} \right)^{m^3} \\ &\quad + O\left(\frac{t^4}{m}\right) + O\left(\frac{t^3}{l}\right). \end{aligned} \quad (\text{A5})$$

By using the substitution $it\hat{A} \rightarrow t^2[\hat{C}, \hat{A}]$ it is also possible analogously to derive

$$\begin{aligned} e^{it^3[\hat{B}, [\hat{C}, \hat{A}]]} &= \left(e^{i\frac{t}{m}\hat{B}} e^{(\frac{t}{m})^2[\hat{C}, \hat{A}]} e^{-i\frac{t}{m}\hat{B}} e^{-(\frac{t}{m})^2[\hat{C}, \hat{A}]} \right)^{m^3} \\ &\quad + O\left(\frac{t^4}{m}, \hat{A}, \hat{B}, \hat{C}\right) \end{aligned} \quad (\text{A6})$$

and finally

$$e^{it^3[\hat{B},[\hat{C},\hat{A}]]} = \left(e^{i\hat{B}\frac{t}{m}} \left(e^{i\hat{A}\frac{t}{ml}} e^{i\hat{C}\frac{t}{ml}} e^{-i\hat{A}\frac{t}{ml}} e^{-i\hat{C}\frac{t}{ml}} \right)^{l^2} e^{-i\hat{B}\frac{t}{m}} \left(e^{-i\hat{A}\frac{t}{ml}} e^{-i\hat{C}\frac{t}{ml}} e^{i\hat{A}\frac{t}{ml}} e^{i\hat{C}\frac{t}{ml}} \right)^{l^2} \right)^{m^3} + O\left(\frac{t^4}{m}\right) + O\left(\frac{t^3}{l}\right), \quad (\text{A7})$$

which we will need in the following. Setting $\tau = t^3$ we finally obtain Eq.(56).

B. Rough estimate of the number of operations needed to implement the cross Kerr evolution

We estimate the order of magnitude of the number of operations that are needed to implement the cross-Kerr evolution given a desired precision y . To provide an estimate, let us focus on the term $e^{\frac{i\tau\hat{p}_1^2\hat{p}_2^2}{4}}$. Taking into account also the Fourier-transform required to implement \hat{p}_1^3 and \hat{p}_2^3 we obtain that in order to implement the nested commutator in Eq.(54) according to Eq.(56) we need to implement

$$[(16l^2 + 6)]m^3 = (y^{-\frac{4}{3}} + 6)y^{-\frac{5}{3}}/36 \sim y^{-3}/36 \quad (\text{B1})$$

elementary operations, where we have only kept the dominant term in $1/y$.

In parallel, from Eq.(56) we see that the typical strength of the evolutions entering the definition of elementary gates will be of the kind

$$\frac{\tau^{1/3}}{ml} \sim \tau^{1/3}\tau^{5/3}\tau^2 = \tau^4 = y^{4/3}. \quad (\text{B2})$$

For precisions of $y = 10^{-3}$ this translates into 10^{-4} .

C. Decomposition of squeezing and beam splitter in elementary gates

For this analysis, we find it simpler to use the symplectic formalism for the elementary gates as introduced in [39]. In this framework, the relevant gates are represented in terms of their action on the quadrature operators as (using the convention $\Delta^2 q_0 = 1/2$ for the vacuum fluctuations)

$$\begin{aligned} \text{Squeezing } e^{-i\frac{\ln s}{2}(\hat{q}\hat{p}+\hat{p}\hat{q})} &\rightarrow \begin{pmatrix} \hat{q}' \\ \hat{p}' \end{pmatrix} = \begin{pmatrix} s & 0 \\ 0 & 1/s \end{pmatrix} \begin{pmatrix} \hat{q} \\ \hat{p} \end{pmatrix} \\ \text{Rotation } e^{i\frac{\theta}{2}(\hat{q}^2+\hat{p}^2)} &\rightarrow \begin{pmatrix} \hat{q}' \\ \hat{p}' \end{pmatrix} = \begin{pmatrix} \cos\theta & -\sin\theta \\ \sin\theta & \cos\theta \end{pmatrix} \begin{pmatrix} \hat{q} \\ \hat{p} \end{pmatrix} \\ \text{Shear } e^{\frac{isq^2}{2}} &\rightarrow \begin{pmatrix} \hat{q}' \\ \hat{p}' \end{pmatrix} = \begin{pmatrix} 1 & 0 \\ s & 1 \end{pmatrix} \begin{pmatrix} \hat{q} \\ \hat{p} \end{pmatrix} \\ \text{FT } e^{\frac{i\pi}{4}(\hat{q}^2+\hat{p}^2)} &\rightarrow \begin{pmatrix} \hat{q}' \\ \hat{p}' \end{pmatrix} = \begin{pmatrix} 0 & -1 \\ 1 & 0 \end{pmatrix} \begin{pmatrix} \hat{q} \\ \hat{p} \end{pmatrix} \end{aligned} \quad (\text{C1})$$

1. Decomposition of the squeezing operator (exact)

We start with the squeezing gate. It is easy to show that

$$\begin{pmatrix} s & 0 \\ 0 & \frac{1}{s} \end{pmatrix} = \begin{pmatrix} 0 & -1 \\ 1 & 0 \end{pmatrix} \begin{pmatrix} 1 & 0 \\ s_3 & 1 \end{pmatrix} \begin{pmatrix} 0 & -1 \\ 1 & 0 \end{pmatrix} \cdot \begin{pmatrix} 1 & 0 \\ s_2 & 1 \end{pmatrix} \begin{pmatrix} 0 & -1 \\ 1 & 0 \end{pmatrix} \begin{pmatrix} 1 & 0 \\ s_1 & 1 \end{pmatrix} \quad (\text{C2})$$

with $s_1 = s, s_2 = 1/s, s_3 = s$. Hence using Eq.(C1) we obtain Eq.(58) of the main text.

2. Decomposition of the beamsplitter operation (exact)

In the proposal of Ref. [22], squeezed cat states undergo a beam splitter transformation that is described by the symplectic matrix

$$\begin{pmatrix} q'_1 \\ q'_2 \end{pmatrix} = \frac{1}{\sqrt{2}} \begin{pmatrix} 1 & 1 \\ 1 & -1 \end{pmatrix} \begin{pmatrix} q_1 \\ q_2 \end{pmatrix}. \quad (\text{C3})$$

We want to decompose this beam splitter gate in terms of elementary gates. We use a procedure inspired by Ref. [40]. For the general change of basis

$$\begin{pmatrix} q'_1 \\ q'_2 \end{pmatrix} = \begin{pmatrix} \sqrt{R} & \sqrt{1-R} \\ \sqrt{1-R} & -\sqrt{R} \end{pmatrix} \begin{pmatrix} q_1 \\ q_2 \end{pmatrix} \equiv M_R \begin{pmatrix} q_1 \\ q_2 \end{pmatrix} \quad (\text{C4})$$

(where the obvious identification $R = 1/2$ allows to retrieve the case of interest of the aforementioned beamsplitter) one has the identity

$$\begin{pmatrix} M_R & 0 \\ 0 & M_R \end{pmatrix} = \left[\begin{pmatrix} 0 & -I_2 \\ I_2 & 0 \end{pmatrix} \cdot \begin{pmatrix} I_2 & 0 \\ M_R & I_2 \end{pmatrix} \right]^3. \quad (\text{C5})$$

This allows us to decompose the beam splitter into Fourier Transform and a gate corresponding to $O(\hat{q}) = e^{i(b_1\hat{q}_1^2+b_2\hat{q}_2^2+b_3\hat{q}_1\hat{q}_2)}$. To discover the correspondence between the coefficients b_1, b_2, b_3 and R we inspect the explicit action of the operator $O(\hat{q})$ on the quadratures:

$$\begin{aligned} e^{-i\hat{q}_1\hat{q}_2b}\hat{p}_1e^{i\hat{q}_1\hat{q}_2b} &= \hat{p}_1 + b\hat{q}_2 \\ e^{-i\hat{q}^2g}\hat{p}e^{i\hat{q}^2g} &= \hat{p} + 2g\hat{q} \end{aligned} \quad (\text{C6})$$

from which it is easy to derive that the operator $O(\hat{q})$ leads to

$$\begin{aligned} \hat{p}_1 &\rightarrow \hat{p}_1 + 2b_1\hat{q}_1 + b_3\hat{q}_2 \\ \hat{p}_2 &\rightarrow \hat{p}_2 + 2b_2\hat{q}_2 + b_3\hat{q}_1. \end{aligned} \quad (\text{C7})$$

This corresponds to the action

$$\begin{pmatrix} \vec{q}' \\ \vec{p}' \end{pmatrix} = \begin{pmatrix} I_2 & 0 \\ M_R & I_2 \end{pmatrix} \begin{pmatrix} \vec{q} \\ \vec{p} \end{pmatrix} \quad (\text{C8})$$

with

$$M_R = \begin{pmatrix} 2b_1 & b_3 \\ b_3 & 2b_2 \end{pmatrix}. \quad (\text{C9})$$

We have hence the identification $b_1 = \sqrt{R}/2, b_2 = -\sqrt{R}/2, b_3 = \sqrt{1-R}$. Hence we finally obtain the decomposition for the beam splitter Eq.(59).

3. Decomposition of the rotation (exact)

For completeness, even though we do not use its expression, we also provide a decomposition of the rotation gate. Due to the identity

$$\begin{pmatrix} \cos \theta & -\sin \theta \\ \sin \theta & \cos \theta \end{pmatrix} = \begin{pmatrix} 0 & -1 \\ 1 & 0 \end{pmatrix} \begin{pmatrix} 1 & 0 \\ s_3 & 1 \end{pmatrix} \begin{pmatrix} 0 & -1 \\ 1 & 0 \end{pmatrix} \\ \cdot \begin{pmatrix} 1 & 0 \\ s_2 & 1 \end{pmatrix} \begin{pmatrix} 0 & -1 \\ 1 & 0 \end{pmatrix} \begin{pmatrix} 1 & 0 \\ s_1 & 1 \end{pmatrix} \quad (\text{C10})$$

with $s_1 = \sec \theta + \tan \theta$, $s_2 = \cos \theta$, $s_3 = \cos \theta + (1 + \sin \theta) \tan \theta$, using Eq.(C1) we conclude that

$$e^{i\frac{\theta}{2}(\hat{q}^2 + \hat{p}^2)} = \hat{F} e^{i\frac{s_3 \hat{q}^2}{2}} \hat{F} e^{i\frac{s_2 \hat{q}^2}{2}} \hat{F} e^{i\frac{s_1 \hat{q}^2}{2}}. \quad (\text{C11})$$

-
- [1] J. ichi Yoshikawa, S. Yokoyama, T. Kaji, C. Sornphiphatphong, Y. Shiozawa, K. Makino, and A. Furusawa, APL Photonics **1**, 060801 (2016), <http://dx.doi.org/10.1063/1.4962732>, URL <http://dx.doi.org/10.1063/1.4962732>.
 - [2] C. M. Wilson, G. Johansson, A. Pourkabirian, M. Simoen, J. R. Johansson, F. Nori, and P. Delsing, Nature **479**, 376 (2011).
 - [3] M. Aspelmeyer, T. J. Kippenberg, and F. Marquardt, Rev. Mod. Phys. **86**, 1391 (2014).
 - [4] O. Houhou, H. Aissaoui, and A. Ferraro, Phys. Rev. A **92**, 063843 (2015).
 - [5] J. Niset, J. Fiurášek, and N. J. Cerf, Phys. Rev. Lett. **102**, 120501 (2009), URL <https://link.aps.org/doi/10.1103/PhysRevLett.102.120501>.
 - [6] R. Namiki, O. Gittsovich, S. Guha, and N. Lütkenhaus, Phys. Rev. A **90**, 062316 (2014), URL <https://link.aps.org/doi/10.1103/PhysRevA.90.062316>.
 - [7] I. L. Chuang, D. W. Leung, and Y. Yamamoto, Phys. Rev. A **56**, 1114 (1997), URL <https://link.aps.org/doi/10.1103/PhysRevA.56.1114>.
 - [8] W. Wasilewski and K. Banaszek, Phys. Rev. A **75**, 042316 (2007), URL <https://link.aps.org/doi/10.1103/PhysRevA.75.042316>.
 - [9] T. C. Ralph, A. J. F. Hayes, and A. Gilchrist, Phys. Rev. Lett. **95**, 100501 (2005), URL <https://link.aps.org/doi/10.1103/PhysRevLett.95.100501>.
 - [10] M. Bergmann and P. van Loock, Phys. Rev. A **94**, 012311 (2016), URL <https://link.aps.org/doi/10.1103/PhysRevA.94.012311>.
 - [11] M. H. Michael, M. Silveri, R. T. Brierley, V. V. Albert, J. Salmilehto, L. Jiang, and S. M. Girvin, Phys. Rev. X **6**, 031006 (2016), URL <https://link.aps.org/doi/10.1103/PhysRevX.6.031006>.
 - [12] Z. Leghtas, G. Kirchmair, B. Vlastakis, R. J. Schoelkopf, M. H. Devoret, and M. Mirrahimi, Phys. Rev. Lett. **111**, 120501 (2013), URL <https://link.aps.org/doi/10.1103/PhysRevLett.111.120501>.
 - [13] M. Mirrahimi, Z. Leghtas, V. V. Albert, S. Touzard, R. J. Schoelkopf, L. Jiang, and M. H. Devoret, New Journal of Physics **16**, 045014 (2014), URL <http://stacks.iop.org/1367-2630/16/i=4/a=045014>.
 - [14] L. Li, C.-L. Zou, V. V. Albert, S. Muralidharan, S. M. Girvin, and L. Jiang, Phys. Rev. Lett. **119**, 030502 (2017), URL <https://link.aps.org/doi/10.1103/PhysRevLett.119.030502>.
 - [15] M. Bergmann and P. van Loock, Phys. Rev. A **94**, 042332 (2016), URL <https://link.aps.org/doi/10.1103/PhysRevA.94.042332>.
 - [16] D. Gottesman, A. Kitaev, and J. Preskill, Phys. Rev. A **64**, 012310 (2001).
 - [17] N. C. Menicucci, Phys. Rev. Lett. **112**, 120504 (2014).
 - [18] T. Douce, D. Markham, E. Kashefi, E. Diamanti, T. Coudreau, P. Milman, P. van Loock, and G. Ferrini, Phys. Rev. Lett. **118**, 070503 (2017).
 - [19] C. Flühmann, V. Negnevitsky, M. Marinelli, and J. P. Home, Phys. Rev. X **8**, 021001 (2018), URL <https://link.aps.org/doi/10.1103/PhysRevX.8.021001>.
 - [20] E. Knill, R. Laflamme, and G. J. Milburn, Nature **409**, 46 (2001).
 - [21] S. Lloyd and S. L. Braunstein, Phys. Rev. Lett. **82**, 1784 (1999).
 - [22] H. M. Vasconcelos, L. Sanz, and S. Glancy, Optics Letters **35**, 3261 (2010).
 - [23] M. G. A. Paris, M. Cola, and R. Bonifacio, Phys. Rev. A **67**, 042104 (2003).
 - [24] A. Bouland, B. Fefferman, C. Nirkhe, and U. Vazirani, arXiv preprint arXiv:1803.04402 (2018).
 - [25] D. Vitali, P. Tombesi, and P. Grangier, Appl. Phys. B **64**, 249 (1997).
 - [26] S. Sefi and P. van Loock, Phys. Rev. Lett. **107**, 170501 (2011).
 - [27] M. Bartkowiak, L.-A. Wu, and A. Miranowicz, J. Phys. B: At. Mol. Opt. Phys. **47**, 145501 (2014).
 - [28] M. Suzuki, Physics Letters A **146**, 319 (1990).
 - [29] H. Yoshida, Physics Letters A **150**, 262 (1990).
 - [30] K. Fukui, A. Tomita, A. Okamoto, and K. Fujii, arXiv:1712.00294 (2018).
 - [31] K. Fukui, A. Tomita, and A. Okamoto, arXiv:1804.04509 (2018).
 - [32] S. Aaronson and A. Arkhipov, Theory of Computing **9**, 143 (2013).
 - [33] E. Farhi and A. W. Harrow, arXiv:1602.07674 (2016).
 - [34] T. Morimae, K. Fujii, and J. F. Fitzsimons, Phys. Rev. Lett. **112**, 130502 (2014).
 - [35] S. Aaronson, *Postbqp postscripts: A confession of mathematical errors*, URL www.scottaaronson.com/blog/?p=2072.
 - [36] K. Fujii and S. Tamate, Scientific Reports **6**, 25598 EP (2016), URL <http://dx.doi.org/10.1038/srep25598>.
 - [37] S. Sefi and P. van Loock, Phys. Rev. A **88**, 012303 (2013).
 - [38] F. Arzani, N. Treps, and G. Ferrini, Phys. Rev. A **95**, 052352 (2017).
 - [39] M. Gu, C. Weedbrook, N. C. Menicucci, T. C. Ralph, and P. van Loock, Phys. Rev. A **79**, 062318 (2009).
 - [40] R. Ukai, Y. J., N. Iwata, P. van Loock, and A. Furusawa,

Phys. Rev. A **81**, 032315 (2010).

- [41] For Bounded Quantum Polynomial time, the class corresponding to the problems we believe could be efficiently solved by a quantum computer.
- [42] Note that we are using inverted notations with respect to Ref. [27]: here in our work ‘1,2’ are used to label the modes and ‘a,b’ the different squeezing parameters.
- [43] Eq.(5) of Ref. [26] is derived with different conventions for the commutator $[\hat{q}, \hat{p}]$ from ours. Therefore, the numerical pre-factor should change. However, due to a missing factor 4 in the numerator of the lhs in Eq.(5) of Ref. [26], that equation is correct within our notations and we can use it as it is.